

AD-A042 913

VON KARMAN INST FOR FLUID DYNAMICS RHODE-SAINT-GENESE--ETC F/G 16/3  
HEAT TRANSFER AND PRESSURE MEASUREMENTS ON A CONCAVE BICONIC MO--ETC(U)  
1977 B E RICHARDS

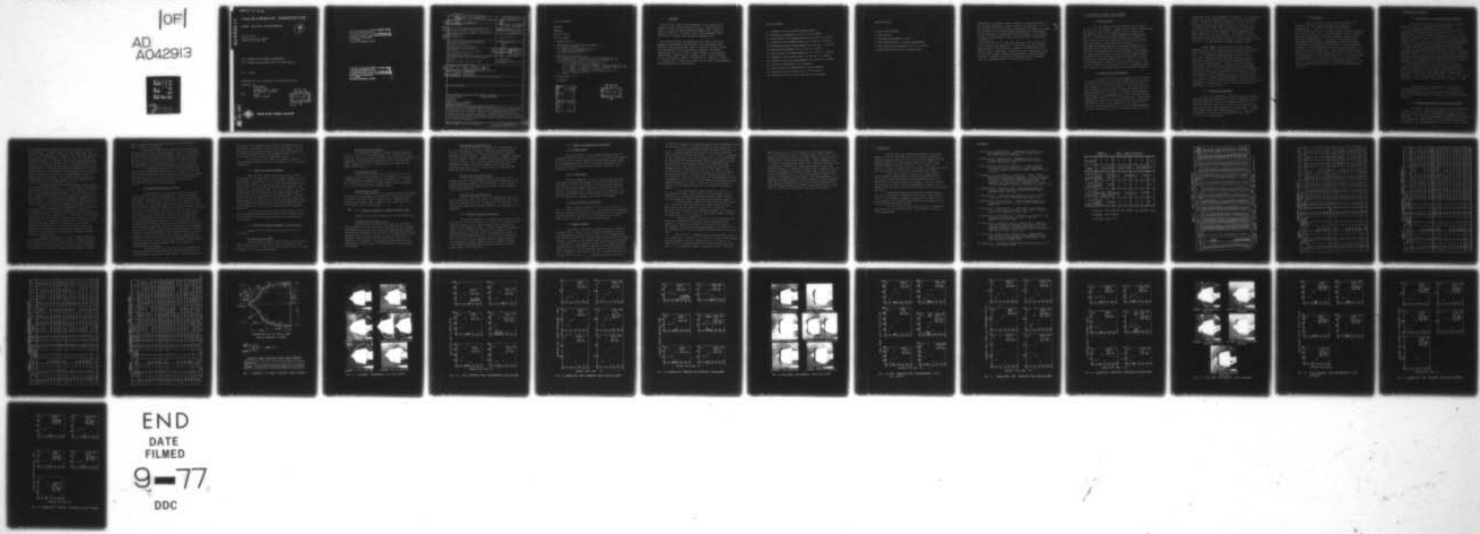
AF-AFOSR-2942-76

AFOSR-TR-77-0845

NL

UNCLASSIFIED

|OF|  
AD  
A042913



END

DATE

FILMED

9-77

DDC



ADA042913

**von KARMAN INSTITUTE  
FOR FLUID DYNAMICS**

9  
P.S.

AFOSR 76-2942  
INTERIM SCIENTIFIC REPORT  
30 NOV 1975-1 DEC 1976

HEAT TRANSFER AND PRESSURE MEASUREMENTS  
ON A CONCAVE BICONIC MODEL WITH FLATTENED NOSETIP

B.E. RICHARDS

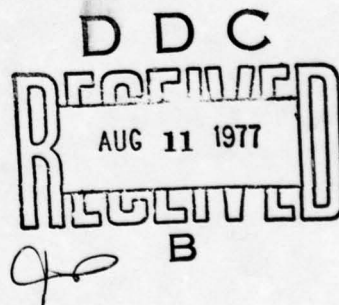
APPROVED FOR PUBLIC RELEASE; DISTRIBUTION UNLIMITED

PREPARED FOR :

SAMSO/RSSE  
PO BOX 92960  
WORLDWAY POSTAL CENTER  
LOS ANGELES, CA 90009

AND

EOARD  
LONDON, ENGLAND



DDC FILE COPY



**RHODE SAINT GENESE BELGIUM**

AIR FORCE OFFICE OF SCIENTIFIC RESEARCH (AFSC)  
NOTICE OF TRANSMITTAL TO DDC  
This technical report has been reviewed and is  
approved for public release IAW AFN 190-12 (7D).  
Distribution is unlimited.  
A. D. BLOSE  
Technical Information Officer

AIR FORCE OFFICE OF SCIENTIFIC RESEARCH (AFSC)  
NOTICE OF TRANSMITTAL TO DDC  
This technical report has been reviewed and is  
approved for public release IAW AFN 190-12 (7D).  
Distribution is unlimited.  
A. D. BLOSE  
Technical Information Officer

## UNCLASSIFIED

SECURITY CLASSIFICATION OF THIS PAGE (When Data Entered)

19 REPORT DOCUMENTATION PAGE			READ INSTRUCTIONS BEFORE COMPLETING FORM
1. REPORT NUMBER 18 AFOSR-TR-77-0845	2. GOVT ACCESSION NO.	3. RECIPIENT'S CATALOG NUMBER 9	
4. TITLE (and Subtitle) 6 HEAT TRANSFER AND PRESSURE MEASUREMENTS ON A CONCAVE BICONIC MODEL WITH FLATTENED NOSETIP.	5. TYPE OF REPORT & PERIOD COVERED INTERIM <i>1st rept.</i> 30 Nov 75 - 1 Dec 76		
7. AUTHOR 10 BRYAN E. RICHARDS	6. PERFORMING ORG. REPORT NUMBER		
9. PERFORMING ORGANIZATION NAME AND ADDRESS VON KARMAN INSTITUTE FOR FLUID DYNAMICS CHAUSSE DE WATERLOO, 72 1640 RHODE-ST. GENEVE, BELGIUM	10. PROGRAM ELEMENT, PROJECT, TASK AREA & WORK UNIT NUMBERS 2307A1 63311F		
11. CONTROLLING OFFICE NAME AND ADDRESS SAMSO/RSSE P O BOX 92060/WORLDWAY POSTAL CENTER LOS ANGELES, CA 90009	12. REPORT DATE 11 12 1977 400		
14. MONITORING AGENCY NAME & ADDRESS (if different from Controlling Office) AIR FORCE OFFICE OF SCIENTIFIC RESEARCH/NA BLDG 410 BOLLING AIR FORCE BASE, D C 20332	13. NUMBER OF PAGES 39		
15. SECURITY CLASS. (of this report) UNCLASSIFIED			
15a. DECLASSIFICATION/DOWNGRADING SCHEDULE			
16. DISTRIBUTION STATEMENT (of this Report) 15 AF-AFOSR-2942-76 Approved for public release; distribution unlimited.			
17. DISTRIBUTION STATEMENT (of the abstract entered in Block 20, if different from Report) 16 2307 17 A1			
18. SUPPLEMENTARY NOTES			
19. KEY WORDS (Continue on reverse side if necessary and identify by block number) HYPERSONIC FLOW SHOCK INTERACTIONS PRE-ENTRY ABLATION HEAT TRANSFER MEASUREMENTS PRESSURE MEASUREMENTS			
20. ABSTRACT (Continue on reverse side if necessary and identify by block number) Heat transfer and pressure measurements have been measured on a concave biconic configuration with a flattened nosetip in the von Karman Institute Longshot free piston tunnel at $M = 15$ and $20$ . The test flow parameters achieved closely simulated re-entry aerodynamic conditions. Information derived from the measurements and also from schlieren photographs enabled statements to be made on the effect of Mach number, Reynold number, surface roughness and flow incidence on the flow over the model.			

LIST OF CONTENTS.

ABSTRACT.

FOREWORD.

LIST OF FIGURES.

LIST OF TABLES.

1. INTRODUCTION.(p. 1)

2. EXPERIMENTAL APPARATUS AND PROCEDURE.(p. 3)

2.1. Test Facility.(p. 3)

2.2. Models and Instrumentation.(p. 3)

2.3. Schlieren photography.(p. 4)

2.4. Test matrix.(p. 5)

3. RESULTS AND DISCUSSION.(p. 6)

3.1. Introduction to the types of flow behaviour.(p. 6)

3.2. Presentation of results and general remarks.(p. 6)

3.3. Detailed discussion of results.(p. 8)

3.3.1. Effect of nosetip roughness.(p. 9)

3.3.2. Effect of surface roughness - zero incidence.(p. 9)

3.3.3. Effect of roughness - angle of attack cases.(p. 10)

3.3.4. Effect of angle of incidence.(p. 11)

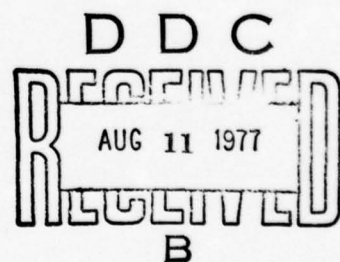
3.3.5. Effect of changing flow conditions.(p. 12)

3.4. Summary comments.(p. 12)

4. CONCLUSIONS.(p. 15)

REFERENCES.

ACCESSION for		
NTIS	White Section <input checked="" type="checkbox"/>	
DDC	Buff Section <input type="checkbox"/>	
UNANNOUNCED	<input type="checkbox"/>	
JUSTIFICATION		
BY _____		
DISTRIBUTION/AVAILABILITY CODES		
Dist.	AVAIL. and/or SPECIAL	
A		-



FOREWORD.

The activities and results documented in this report were supported under project 63311F with Cap. J. Green and Lt. E. Taylor of Space and Missile Systems Organization, acting as project engineers. The report covers work conducted during the period 1 December 1975 through 30 November 1976.

The technical advice and guidance by Mr. Victor DiCristina, Manager, Thermodynamics and Materials Test Department, Avco Systems Division, Wilmington, Mass in the area of model design and instrumentation was particularly valuable: The author acknowledges the help of Mssrs. Roger Connaselle and Fernand Vandenbroek in operating the longshot and Mr. Jean-Claud Lobet for the photography. Mssrs. M. Kenworthy, P. Labour, B. Daval, G. Capaldi, and I. Hodge participated in the tests, data reduction, and interpretation of the results.

LIST OF FIGURES.

1. Schematic of blunt concave biconic model J.
- 2a. Schlieren photographs,  $M = 16$ ,  $Re = 9 \times 10^6/\text{ft.}$
- 2b. Heat transfer rate measurements,  $M = 16$ ,  $Re = 9 \times 10^6/\text{ft.}$
- 2c. Normalized heat transfer rate,  $M = 16$ ,  $Re = 9 \times 10^6/\text{ft.}$
- 2d. Normalized pressure measurements,  $M = 16$ ,  $Re = 9 \times 10^6/\text{ft.}$
- 3a. Schlieren photographs,  $M = 20$ ,  $Re = 3 \times 10^6/\text{ft.}$
- 3b. Heat transfer rate measurements,  $M = 20$ ,  $Re = 3 \times 10^6/\text{ft.}$
- 3c. Normalized heat transfer rate,  $M = 20$ ,  $Re = 3 \times 10^6/\text{ft.}$
- 3d. Normalized pressure measurements,  $M = 20$ ,  $Re = 3 \times 10^6/\text{ft.}$
- 4a. Schlieren photographs, zero incidence.
- 4b. Heat transfer rate measurements, zero incidence.
- 4c. Normalized heat transfer rate, zero incidence.
- 4d. Normalized pressure distributions, zero incidence.

LIST OF TABLES.

1. Test identification.
2. Test matrix.
3. Pressure measurements,  $\text{lb/in}^2$ .
4. Non-dimensionalised pressure measurements.
5. Heat transfer measurements (B. Th. U./ $\text{ft}^2 \text{sec}$ ).
6. Non-dimensionalised heat transfer rates.

measurements on concave biconic surfaces in steady flow (Ref. 8) and unsteady pressures on concave concic surfaces (Ref. 9). In all of these studies the level of achievement has been in checking the feasibility of the measurement technique and to developing initial analyses to explain the results obtained. Some further analyses of the results, however, have been made by DiCristina et al(Ref. 10).

The present series of test, the results of which are here reported, concern the completion of the studies on heat transfer measurements on concave biconic surfaces in steady flow, commenced in Ref. 8 and deals in particular with a methodical study of the effect of Mach number, Reynold number, surface roughness and model incidence on this model shape but with a flattened nose tip, designated model J in these last series.

## 2. EXPERIMENTAL APPARATUS AND PROCEDURE.

---

### 2.1 Test facility.

The von Karman Institute Longshot test facility was used for this program. Longshot differs from a conventional gun tunnel in that heavy piston is used to compress the nitrogen test gas to very high pressures and temperatures (Ref. 1). The test gas is then trapped in a reservoir at peak conditions by the closing of a system of check valves. The flow conditions decay monotonically during 10 to 20 milliseconds running times as the nitrogen trapped in the reservoir flows through the 6° half-angle conical nozzle into the pre-evacuated open jet test chamber. The extremes in supply conditions used in these tests are approximately 55,000 lb/in<sup>2</sup> at 1900°K and 38,000 lb/in<sup>2</sup> at 2320°K. These provide unit Reynolds numbers of  $8.5 \times 10^6$  and  $2 \times 10^6$  per ft at nominal Mach numbers of 15 and 20 respectively. The two Mach numbers were obtained at the 14 in. diameter nozzle exit plane by using throat inserts with different diameters.

### 2.2 Models and instrumentation.

The concave biconic model supplied by Avco Systems Division, consisted of a concave forebody which is smoothly faired into 14° half-angle conical after body which has a base diameter of 6.25 in (see Fig. 1). The model radius at the forebody-afterbody junction (referred to later as the model shoulder) was 2.187 ins. The radius of the generator defining the concave forebody was 2.75 in. giving a surface angle change from 24° to 70° to the model axis. Three interchangeable nose tips were supplied by Avco. One, designated nose-tip "H" had a 0.312 in spherical tip, nose-tip "I" was a 20° half-angle cone with a 0.125 in radius hemispherical tip, nose-tip "J" of a 0.4 in extension with a 1.5 in

R spherical nose. The designation of models H, I, J, was given to the basic model fitted with each of the nose tips respectively. Model J(R) consisted of Model J in which the 1.5 in R stagnation region was roughened with metal chips of 0.02 in average size. Model J(R)' consisted of this same model but with the whole of the concave surface roughened with metal spheres of 0.065 in diameter. Photographs of these latter two models are shown in Fig. 2. of Ref. 8. The tests described in this report are carried out only on Models J, J(R) and J(R)', but some reference is made to Models H and I.

Eight copper calorimeter heat transfer gauges manufactured by BBN and supplied with the models were mounted flush axially along the model surface as illustrated in Fig. 1. An additional gouge was placed on the nose of the model. Eight pressure taps were identically spaced along the surface but at  $180^\circ$  around the model from the row of heat transfer gauges. Details of the heat sensors used, their calibration and associated recording equipment is given in Ref. 3. The calibration constants, are determined over a heat flux range from 20 to 80 B Th U/ft<sup>2</sup> sec in the AEDC radiant heat flux calibration facility before mounting in the model. Steady pressure measurements on these models were made using Hidyne variable reluctance and PCB piezoelectric transducers. A description of them, their calibration and application is given in Ref. 3.

### 2.3. Schlieren photography.

An 18 in conventional single pass Toepler schlieren system equipped with high quality optical components is used. With the exception of one 24 in diameter plane mirror to bend the light  $90^\circ$  (due to the vicinity of a wall near the test section) the light beam takes a Z-shaped path. A single spark light source with a spark duration of 1 sec is used in some test to record the visualisation of the flow on 3 1/4 x 4 1/4 in sheet film.

#### 2.4 Test Matrix.

Table 1 gives the scope of the test series and identifies the test number with each model and flow configuration. It can be seen that the test series provides cross sections of a complete matrix involving the parameters of flow Mach number, Reynolds number, surface roughness and angle of incidence. The test conditions given in this table are nominal values. The actual test conditions were calculated from appropriate measurements using the Longshot data reduction programme (obtained in Ref. 3) and summarised in Table 2. The test numbers after 549 were those carried out within the present grant period. Earlier tests numbers were carried out in an earlier grant period (Ref. 8) and are included for completeness. In the latter case not all the test provided complete information; but were included since they filled in data for tests in which there were instrument failure, or since more information was required to clarify the understanding of the flow.

### 3. RESULTS AND DISCUSSION.

#### 3.1 Introduction to the types of flow behaviour.

The flow over concave conic body shapes similar to model J is likely to fall into three categories:

i) The "high drag steady inviscid flow" so-called from a study concerning tension shell re-entry shapes (Ref. 11). This involves a weak bow shock that interacts with a strong shoulder shock with little or no separation: The flow was described in detail in Ref. 8. The high drag is caused by the development of very large surface pressures caused by efficient isentropic compression on forward facing concave surfaces.

ii) The "low drag steady separated flow" in which large separated regions occur starting near the nose and re-attaching near the shoulder. In this case the large pressures created in the first flow configuration are suppressed by the displacement thickness of the separated flow, causing an effective "streamlining" of the surfaces at large angles to the flow.

iii) The "pulsating" flow, in which there is a dramatic excursion between two very different shock envelopes, the inner one resembling the high drag steady inviscid flow, and the other a single bow shock surrounding the whole body. Examples of such a flow are given in Refs. 9, 11. Up to present this type of flow has never been detected on models H, I and J.

Various facets of these types of flow have been discussed in detail in Refs. 8, 9, 10, 11. A criterion for determining whether the flow will be "high drag steady flow" or "low drag steady or pulsating flow" has been discussed in Ref. 10.

#### 3.2 Presentation of Results and General Remarks.

The overall basic results of the study are presented in Figs. 2, 3 and 4. These are displayed in such a way as to facilitate the discussion of the effects of changing various parameters. The schlieren photographs, dimensional heat transfer rate, normalised heat transfer rate and normalised pressure are given in the figures designated a, b, c, d. Fig. 2 presents

the results taken on models J and J(R)' at nominal condition of  $M=16$  and  $Re=9 \times 10^6$  per ft; Fig. 3 gives those on the same models at  $M=20$  and  $Re=3 \times 10^6$  per ft. The final Fig. 4 presents the results on these models at  $M=16$  and  $Re=4.5 \times 10^6$  per ft. and  $M=20$  and  $Re=2 \times 10^6$  per ft. and the only test made at  $M=20$  and  $Re=3 \times 10^6$  per ft. on Model J(R). The approximate position of the shock intersection and related interaction region as determined from the schlieren pictures are denoted by a vertical shaded region in those figures. The forward part of the shaded region denotes the position of the extrapolation of the aft shock to the model surface. The rearward position denotes the intersection with the model surface of a line drawn from the shock intersection in a streamwise direction.

The experimental and normalised results for all tests are also presented in Tables 3 - 6. The pressures are normalised with respect to the pitot pressure, which is assumed to be the same as the stagnation point pressure. The heat transfer rates are normalised with respect to the theoretical stagnation point heat transfer on a 0.312 in radius hemisphere, whose value is given in Table 2, and which is calculated from freestream conditions using the Fay and Riddel formula as presented in Ref. 3.

Because of model and instrumentation size limitations, and number of recording channels available, the density of instrumentation was not high considering the very high gradients in pressure and heat transfer rates. The result of this is that interpretation of the results is sometimes difficult. On close examination of the assembled results, there is a good case for stating that gauge number 3 is reading high in all tests. Pending re-calibration of this gauge, the value of the heat transfer rate at position 3 was mentally decreased by about 30% in the interpretation of the results, although the actual reduced data was plotted.

A negative incidence,  $\alpha$ , in the figures represents a "leeward" surface and a positive value a "windward" surface. Since during one particular test, the heat transfer gauges are on a windward surface when the pressure taps are on a leeward surface and vice versa, the figures are re-arranged to align

data on surfaces with the same attitude to the flow rather than in terms of run numbers.

An important observation concerns the sensitivity of the flow field to very small incidences. This is illustrated by examining the schlieren photographs in Figs. 3 iv) (Run 557) and 4 iv) (Run 556) which showed asymmetry of the shock wave patterns for an incidence of the order of 20' which is within the resolution of the incidence gear used. This in turn has a large effect on the pressure and heat transfer distributions.

It is pointed out also that for the rough model, the heat transfer gauges and pressure taps lie below the mean surface, and may be sensing local interaction caused by the roughness elements themselves. It is hence expected that the results on the rough surfaced models will be more scattered and less accurate than those as the smooth models.

### 3.3 Detailed discussion of results.

On examination of the schlieren pictures it is seen that all but one of the test carried out on these flattened nose models resulted in "low drag steady flow" to be generated (although on the "windward" side of some of the angle of attack tests, signs of high drag steady invisiid flow" are seen). For these cases the separated region is so extensive that the separated point can be considered to be fixed close to the nose (i.e. in the region of the shoulder at the nose), and the interesting feature then lies in the position of the reattachment point. This re-attachment location and the after or shoulder shock are mutually dependent, because it is the interaction of the shoulder shock with the foreshock that contributes to the significant pressure gradients needed for separation to be triggered, and yet this shoulder shock is likely to be connected with the position of flow re-attachment where high speed flow is turned sharply to follow the contour of the surface. The detailed analysis of the flow field for these large separated flow cases is beyond the scope of this work, but the effect of Mach number, Reynolds number, surface roughness and flow incidence is qualitatively illustrated.

A rough idea as to the position of re-attachment was determined from the observation that the shock wave above the concave surface was usually quite conical. Hence the displace-

ment angle of the separate flow could be assessed using cone tables and a measurement of the conical shock angle. A line was then drawn from the shoulder of the nose at the angle of the assessed separated flow displacement thickness until it cut the surface at the supposed re-attachment point.

A discussion of the effect of separate changes in flow and model configuration will be presented in the following subsections.

### 3.3.1 Effect of nosetip roughness.

Only one test, number 532 at  $M=16$ ,  $Re=3 \times 10^6/\text{in}$ , was carried out on model J(R), which included roughness only on the nosetip. This turned out to be the only configuration in these tests on model J and its derivatives at zero angle of attack in which the high drag inviscid flow case appeared. The results are illustrated in Figs. 4(v) a, b, c, and d. The peak pressure and heat transfer occur just before gauge number 3. At the same test flow conditions, the smooth model J (run 529) and the fully rough model J(R)' (runs 533 and 557) showed low drag separated flow with peak conditions occurring between gauges 3 and 4, peak heat transfer rates both being slightly lower than on model J(R). No conclusion is made on this unexpected behaviour.

In any future tests on these concave biconic models, it is strongly recommended that further tests be made on model J(R) at higher and lower Reynolds number to help understand this behaviour.

### 3.3.2 Effect of surface roughness - zero incidence.

Examples of this effect were studied at all flow conditions.

$$M = 16, Re = 9 \times 10^6/\text{ft}.$$

No perceptible change in shock position, heat transfer level or pressure level was seen at this flow condition (see Figs. 2 ii and 2 iii). The level of heat transfer rate is slightly higher in the rough surfaced model.

$$M = 16, Re = 4.5 \times 10^6/\text{ft.}$$

No perceptible change in shock position or pressure level was seen, but the heat transfer rate distribution indicates the interaction occurring further forward with the addition of roughness as indicated by the position of the heat transfer peak. Generally the heat transfer levels are higher on the rough surfaced model.

$$M = 20, Re = 3 \times 10^6.$$

The bow shock position lies further out due to the roughness causing the interaction to be delayed. This causes a delayed peaks in pressure and heat transfer rates. Overall heat transfer to the body is slightly decreased with roughness due to a low heating on the shoulder gauge.

$$M = 20, Re = 2 \times 10^6.$$

The bow shock position lies slightly further out causing interaction to be delayed. No perceptible change in position of pressure and heat transfer peak is seen. Slightly lower overall heat transfer rate is found on the rough model due to a low value on the shoulder gauge.

### 3.3.3 Effect of roughness - angle of attack cases.

Examples of this were examined at two flow conditions.

$$M = 16, Re = 9 \times 10^6, \quad = -3.$$

In both smooth and rough wall cases the separated flow reattaches near the shoulder as indicated by the schlieren photographs and the relatively flat pressure and heat transfer distributions upstream of the shoulder. The pressure peaks just upstream of the shoulder, whilst the heat transfer peaks at the shoulder. Both the heat transfer and pressure levels are increased due to roughness. On the smooth model only the bow shock wave is present, with no perturbation seen arising from the shoulder.

$$M = 20, Re = 3 \times 10^6, \alpha = -3.$$

The bow shock wave is closer to the surface than at  $M = 15$ , resulting in an earlier interaction, with resulting earlier re-attachment as evidence from the earlier peaks in pressure and heat transfer. Pressure level is slightly increased and heat transfer level is slightly decreased by adding roughness to the model. The schlieren picture indicates that the interaction between the shocks changes little with added roughness, and this effect is reflected in the pressure and heat transfer distributions.

$$M = 16, Re = 9 \times 10^6, \alpha = +3.$$

In this case roughness causes a very distinctive movement of the bow shock towards the model surface with a subsequent upstream movement of the interaction. Heat transfer and pressure peaks and overall heat transfer to the surface is little changed however.

$$M = 20, Re = 3 \times 10^6, \alpha = +3.$$

Again in this case, there is a movement of the bow shock towards the body, but this is less distinctive than in the last case because the shock is already close to the wall. The overall heat transfer to the wall appears to be decreased by roughness.

### 3.3.4 Effect of angle of incidence.

Two flow situations or two models were tested to study this effect. The chief effect in all cases is to increase the separated region on the leeward surface and to decrease the region on the windward surface. The heat transfer and pressure peaks tend to be lower and closer to the shoulder on the leeward surface, and higher, more concentrated and closer to the nose on the windward surface. In the case of the Mach 20,  $Re = 3 \times 10^6$  test, it is apparent that the separated region is suppressed or mainly suppressed on the windward surface. It is evident hence that small incidence changes cause very large changes of flow behaviour.

### 3.3.5 Effect of changing flow conditions.

#### $\alpha = 0$ , smooth model.

From examination of the schlieren pictures there is a distinct trend that the bow shock wave moves away from the surface with decreasing Mach number and decreasing Reynolds number. The accompanying trend of more concentrated and higher values of heat transfer and pressure with movement forward of the interaction occurs.

#### $\alpha = 0$ , rough model.

The same comments, as for the smooth model are applicable here, although the changes are much less significant. The general trend of the bow shock wave further from the wall for the rough body situation generally reflects the trend of increase of boundary layer thickness due to the roughness. The physical modification of the model dimensions due to the addition of significant roughness should not be discounted.

#### $\alpha = \pm 3$ , smooth and rough models.

Only a change from  $M = 16$ ,  $Re = 9 \times 10^6$  to  $M = 20$ ,  $Re = 3 \times 10^6$  was made in this case. Schlieren pictures, pressure and heat transfer distributions illustrated that the interaction moves forward with the change from the former to the latter conditions in line with the zero incidence cases.

### 3.4 Summary comments.

From these comparisons, a general pattern of results becomes evident. First of all, from the information that the non-dimensionalized heat transfer levels do not change greatly over the whole test series indicate that the flow over the concave surface is unlikely to be laminar, and is either fully turbulent or transitional. This conclusion also could be drawn from the observation that the separated regions, as ascertained approximately from the position of the bow shock wave, do not vary in size considerably, and that for the cases in which laminar flow is most likely to exist (i.e. high Mach number cases, with

low Reynolds numbers) the separated regions are the smallest, which is contrary to what is expected of laminar flow separation.

The heat transfer and pressure distribution on the surface is largely dominated by the position of the interaction of the shock waves above the surface. The aft shock is connected to the re-attachment point by its appearing to be an extension of the strong shock wave generated near re-attachment necessary to deflect the flow initially outside the separated region along the wall. The results of the interaction cause heat transfer rates and pressures to peak in this region. When the interaction occurs early on the body, the result is higher and more concentrated (or peaky) heat transfer and pressure distributions. When this occurs late, the distributions are less concentrated, and if very late the effects are attenuated by the expansion around the corner. These effects should be kept in mind in the following discussion of the effects of parameter change.

Increasing Reynolds numbers appears to move the interaction upstream. This aligns with the frequently found behaviour of a transitional separated boundary layer that increasing Reynolds numbers causes decreased separated length.

Increasing Mach number also appears to move the interaction forward. This aligns with the usual trend that high Mach number boundary layers are more robust to pressure gradients with the result that separated lengths are decreased. The shock layer is also thinner at higher Mach numbers helping to advance the shock intersection.

Increase of angle of the flow to the surface has the effect of bringing the interaction zone forward, and the opposite is true for a decrease in the angle of the flow to the surface. These trends are associated with the movement of the highest positive pressure gradients forward and aft, respectively:

The effect of roughness on the surface varies with flow conditions. At Mach 16,  $\alpha = 0$  and  $\alpha = -3$  cases little change in flow behaviour is seen. At Mach 20, for  $\alpha = 0$  and  $\alpha = -3$  cases, there is a general tendency for the interaction to move aft, i.e. the separation region to increase in size. For both

Mach numbers, at  $\alpha = +3$  the interaction zone moves forward. It is striking that in the literature there exists little information on separated flows on rough surfaces to guide the interpretation of these complicated flows. Since roughness has the effect of advancing the onset of the turbulent boundary layer in laminar and transitional flows then separated length are likely to decrease. In fully turbulent flows, roughness has the effect of thickening a turbulent boundary layer and it has been shown for example in Ref. 12 that the separation length is increased by a thickened boundary layer. One interpretation of the phenomena mentioned earlier in this paragraph is that separated flows which are already extensive on the smooth bodies will be controlled by the thickened boundary layer effect, whilst those which are short are influenced by the transition effect.

#### 4. CONCLUSIONS.

Pressure and heat transfer measurements and visualization of the flow were made on a concave biconic shape with a flattened nosetip tested in the flow of the von Karman Institute Longshot facility at nominal Mach numbers of 16 and 20 and Reynolds numbers from  $9.0 \times 10^6$  and  $4.5 \times 10^6$  and  $3.0 \times 10^6$  and  $2.0 \times 10^6$  per ft respectively. The effect of surface roughness and flow incidence of  $\pm 3^\circ$  on the measurements was studied.

In all flow cases but with the wall either smooth or fully roughened, large separated regions were developed over the concave surface resulting in the interaction of the bow shock with the shoulder shock to occur late. For the only test on the model with just the nosetip roughened, little or no separation was developed with the result that the shock interaction was early.

Increasing Reynolds number and Mach number advances the shock interaction. Roughness tends to have little effect at  $M = 16$  but slightly retards the interaction at Mach 20, for zero incidence and "leeward" flow surfaces, but advances the interaction for "windward" surfaces.

Early interaction causes higher and more concentrated pressures and heat transfer rates. The reverse is true for late interactions.

REFERENCES.

1. Richards B.E., Enkenhus K.R. : "Hypersonic testing in the VKI Longshot piston tunnel", AIAA Journal, Vol.8, N°6, June 1970, pp. 1020-1025.
2. Richards B.E., Enkenhus K.R. : "Stagnation point heat transfer and pressure distribution on a hemisphere at  $M=15$ ", VKI TR 39, 1970.
3. Richards B.E., Culotta S., Slechten, J. : "Heat transfer and pressure distributions on re-entry nose-shapes in the VKI Longshot hypersonic tunnel", AFML-TR-71-200, June 1971.
4. Richards B.E., DiCristina V., Minges M.L. : "Heat transfer and pressure distribution on sharp and finite bluntness biconic and hemispherical geometries at various angles of attack in a Mach 15-20 flow", Astronautical Research, 1971, edited by L.G. Napolitano, D. Reidel, Publishing Company, Dordrecht, Holland, 1973, pp. 91-103.
5. Richards B.E. : "Hypersonic heat transfer measurements on re-entry vehicle surfaces at high Reynolds number", AFML-TR-73-187, June 1973.
6. Richards B.E. : "Boundary layer transition on blunt bodies in hypersonic flow", AFML-TR-75-139, Sept. 1975.
7. Richards B.E., Kenworthy M.A. : "Pressure measurements on a convex biconic model in a Mach 15 flow", VKI TR 84, March 1974.
8. Richards B.E., Kenworthy M.A. : "The study of the effect of shock interaction on concave conic shapes in hypersonic flow", AFML-TR-137, Sept 1975.
9. Kenworthy M.A., Richards B.E. : "A study of the unsteady flow over concave conic model at Mach 15 and 20". AFML-TR-75-138, Sept 1975.
10. DiCristina V., Chen K.K., Lin T., and Liu T.M. : "Exploratory development of hypersonic heat transfer and thermochemical ablation of advanced materials : nosetip test data evaluation and rough wall transition analysis." AFML-TR-75-25, Vcl.1, April 1975.
11. Jones R.A., Bushnell D.M., and Hunt J.L. : "Experimental flow field and heat transfer investigation of several tension shell configurations at a Mach number of 8". NASA. TN-D-3800, January 1967.
12. Appels, C. : "Turbulent boundary layer separation at Mach 12". V.K.I. TN 90, Sept. 1973.

TABLE 1 TEST IDENTIFICATION

Incidence											Fig.
Model	J	J(R)	J(R)'	J	J(R)	J(R)'	J	J(R)	J(R)'	No.	
$M = 16^*$ $Re = 9 \times 10^6$	531 <sup>†</sup> 536°	-	534 561	551	-	553	552	-	554	2	
$M = 16^*$ $Re = 5 \times 10^6$	530 537°	-	560	-	-	-	-	-	-	4	
$M = 20^*$ $Re = 3 \times 10^6$	529	532 (Fig 4)	533 557	549	-	558	550	-	559	3	
$M = 20^*$ $Re = 2 \times 10^6$	535 539	-	556	-	-	-	-	-	-	4	

\* nominal test conditions, see Table 2 for measured values

† Longshot test number

° Schlieren picture only.

TABLE 2. TEST MATRIX AND CONDITIONS

RUN	MODEL	INCLD. (deg)	$P_o$ (lb/in <sup>2</sup> )	$P_o$ (lb/in <sup>2</sup> )	$T_o$ (K)	$T_o$ perf. (K)	$T_{1,2}$ (K)	$M$	$Re \times 10^6$ (ft <sup>-1</sup> )	$T$ (K)	$T_{wind}$ (K)	V (ft/sec)	$Q^+$ (BTU/ft <sup>2</sup> sec)
529	J	0	62,800	78,500	2350	3060	2680	7.23	20.7	3.1	1.29	35.3	8230
530	J	0	34,700	39,100	2020	2470	2200	13.6	15.6	4.5	4.44	40.4	234
531	J	0	60,900	93,400	1904	2500	2230	22.2	16.8	8.6	6.38	43.4	42.1
532	J(Q)	0	58,500	70,100	2350	3030	2660	6.5	20.6	2.8	1.20	35.2	35.1
533	J(Q)	0	63,300	79,600	2350	3060	2680	7.20	20.8	3.1	1.27	35.0	35.0
534*	J(Q)	0	60,900	93,400	1904	2500	2230	22.2	16.8	8.6	6.38	43.4	42.1
535	J	0	40,000	42,00	2320	2878	2533	4.8	19.9	2.03	0.92	36.0	34.2
536	J	0	59,200	89,600	1900	2480	2210	22.50	16.9	8.4	6.06	42.9	41.9
537	J	0	38,300	44,600	2030	2500	2230	15.52	15.8	4.9	4.78	49.2	40.1
539	J	0	41,100	43,300	2350	2920	2565	4.75	20.0	2.0	0.91	36.1	34.1
549	J	±3	58,000	69,400	2370	3050	2670	7.71	19.7	3.0	1.49	37.9	35.9
550	J	±3	61,400	74,700	2390	3000	2710	8.99	19.6	3.3	1.79	39.8	36.5
551	J	±3	54,200	74,800	1910	2460	2200	24.2	16.1	8.3	7.13	46.4	42.5
552	J	±3	58,700	87,800	1910	2500	2230	26.8	16.2	9.0	7.84	46.7	42.7
553	J(Q)	±3	54,700	85,800	1900	2480	2210	23.5	16.6	8.4	6.56	44.3	42.0
554	J(Q)	±3	57,100	84,600	1900	2470	2210	26.3	16.1	8.9	7.74	46.6	42.8
556	J(Q)	0	47,300	50,000	2460	3100	2710	5.54	19.9	2.1	1.07	38.5	34.5
557	J(Q)	0	67,100	85,600	2380	3130	2730	7.91	20.7	3.2	1.42	36.1	35.5
558	J(Q)	±3	66,100	83,300	2390	3140	2740	7.75	20.7	3.1	1.39	36.3	35.4
559	J(Q)	±3	66,300	83,800	2390	3130	2740	8.02	20.5	3.2	1.46	36.7	35.6
560	J(Q)	0	37,200	43,100	1980	2430	2174	14.6	15.9	4.9	4.46	47.3	40.3
561	J(R)	0	61,900	95,500	1912	2521	2244	22.7	17.1	8.5	5.97	42.6	41.6

\* incomplete free stream data taken from Run 531  
+ theoretical stagnation point heat transfer on 0.312 in radius hemisphere (Avco Model H).

TABLE 3 PRESSURE MEASUREMENTS ( $lb/in^2$ )

M	$D_a \times 10^{-6}$ ft <sup>-1</sup>	Model	Incidence (degrees)	Rum No	Pitot pressure	Stagnation 1	2	3	4	5	6	7	8
16.8	8.6	J	0	531	22.2	12.6	12.9	15.9	24.3	7.1	1.3	1.6	1.9
16.2	9.0	J	+3	552	26.8	15.8	13.9	15.1	26.1	6.1	1.1	2.4	2.9
16.1	8.3	J	-3	551	24.2	17.7	13.8	12.8	15.3	-	1.4	1.2	1.4
16.8	8.6	J(Q)	0	534	22.2	14.2	14.4	18.5	24.0	-	1.3	1.5	2.1
17.0	8.5	J(Q)	0	561	23.0	12.9	14.8	12.0	15.1	10.3	1.6	1.2	1.4
16.1	8.9	J(Q)	+3	554	26.3	13.4	14.0	17.1	25.5	5.3	1.7	2.4	2.7
16.4	8.4	J(Q)	-3	553	23.5	14.2	14.0	13.7	20.7	9.7	1.4	1.4	1.7
15.6	4.5	J	0	530	15.5	8.1	8.6	12.9	13.6	9.6	0.8	1.0	1.2
15.9	4.9	J(Q)	0	560	14.6	8.5	10.3	8.9	11.7	5.5	1.1	0.8	1.1
20.7	3.1	J	0	529	7.2	3.9	3.6	5.1	14.5	-	0.4	0.6	0.5
19.6	3.3	J	+3	550	9.0	3.6	4.2	7.4	7.7	1.9	0.48	0.66	0.61
19.9	3.0	J	-3	549	7.7	3.2	3.7	3.8	4.6	2.9	0.46	0.40	0.45
20.8	3.1	J(Q)	0	533	7.2	3.9	4.0	5.9	9.2	3.5	0.3	0.5	0.7
20.7	3.2	J(Q)	0	557	7.9	3.4	5.2	4.1	5.6	3.4	0.4	0.4	0.6
20.5	3.2	J(Q)	+3	559	8.0	3.2	5.5	6.0	9.7	1.7	0.7	0.6	0.7
20.7	3.1	J(Q)	-3	558	7.8	3.3	4.9	4.3	5.7	2.7	0.5	0.4	0.4
20.6	2.8	J(Q)	0	532	6.5	2.1	6.4	10.2	7.8	1.6	0.5	0.7	0.6
19.9	2.0	J	0	535	4.8	2.6	2.5	3.7	5.9	2.0	0.3	0.4	0.4
19.9	2.1	J(Q)	0	556	5.5	2.6	2.7	2.8	3.5	2.2	0.4	0.3	0.3

TABLE 4. NON-DIMENSIONALISED PRESSURE MEASUREMENTS

M	$Re \times 10^{-6}$	Model	Incidence (degrees)	Run No	Distor pressure	Gauge 1	2	3	4	5	6	7	8
16.8	8.6	J	0	531	1.0	0.57	0.58	0.71	1.07	0.32	0.06	0.07	0.09
16.2	9.0	J	+3	552	1.0	0.59	0.52	0.58	0.94	0.23	0.04	0.09	0.11
16.1	8.3	J	-3	551	1.0	0.73	0.57	0.53	0.63	-	0.06	0.05	0.06
16.8	8.6	J( $\alpha$ )'	0	534	1.0	0.64	0.65	0.84	1.10	-	0.06	0.07	0.09
17.0	8.5	J( $\alpha$ )'	0	561	1.0	0.56	0.64	0.52	0.65	0.45	0.07	0.05	0.06
16.1	8.9	J( $\alpha$ )'	+3	554	1.0	0.51	0.53	0.65	0.97	0.20	0.07	0.09	0.10
16.4	8.4	J( $\alpha$ )'	-3	553	1.0	0.61	0.60	0.58	0.88	0.41	0.06	0.06	0.07
15.6	4.5	J	0	530/537	1.0	0.59	0.63	0.83	0.87	0.62	0.06	0.07	0.09
15.9	4.9	J( $\alpha$ )'	0	560	1.0	0.58	0.70	0.61	0.80	0.38	0.08	0.05	0.08
20.7	3.1	J	0	529	1.0	0.54	0.50	0.71	2.0	-	0.06	0.09	0.07
19.6	3.3	J	+3	550	1.0	0.39	0.47	0.83	0.86	0.21	0.05	0.07	0.07
19.9	3.0	J	-3	549	1.0	0.42	0.47	0.50	0.59	0.38	0.06	0.05	0.06
20.8	3.1	J( $\alpha$ )'	0	533	1.0	0.54	0.56	0.82	1.28	0.49	0.04	0.07	0.10
20.7	3.2	J( $\alpha$ )'	0	557	1.0	0.43	0.66	0.52	0.71	0.43	0.05	0.05	0.08
20.5	3.2	J( $\alpha$ )'	+3	559	1.0	0.40	0.69	0.75	1.21	0.20	0.06	0.07	0.09
20.7	3.1	J( $\alpha$ )'	-3	558	1.0	0.42	0.63	0.55	0.73	0.35	0.07	0.05	0.06
20.6	2.8	J( $\alpha$ )	0	532	1.0	0.32	0.99	1.57	1.20	0.25	0.07	0.10	0.10
19.9	2.0	J	0	535	1.0	0.54	0.52	0.77	1.23	0.42	0.06	0.07	0.08
19.9	2.1	J( $\alpha$ )'	0	556	1.0	0.47	0.49	0.51	0.64	0.4	0.07	0.05	0.06

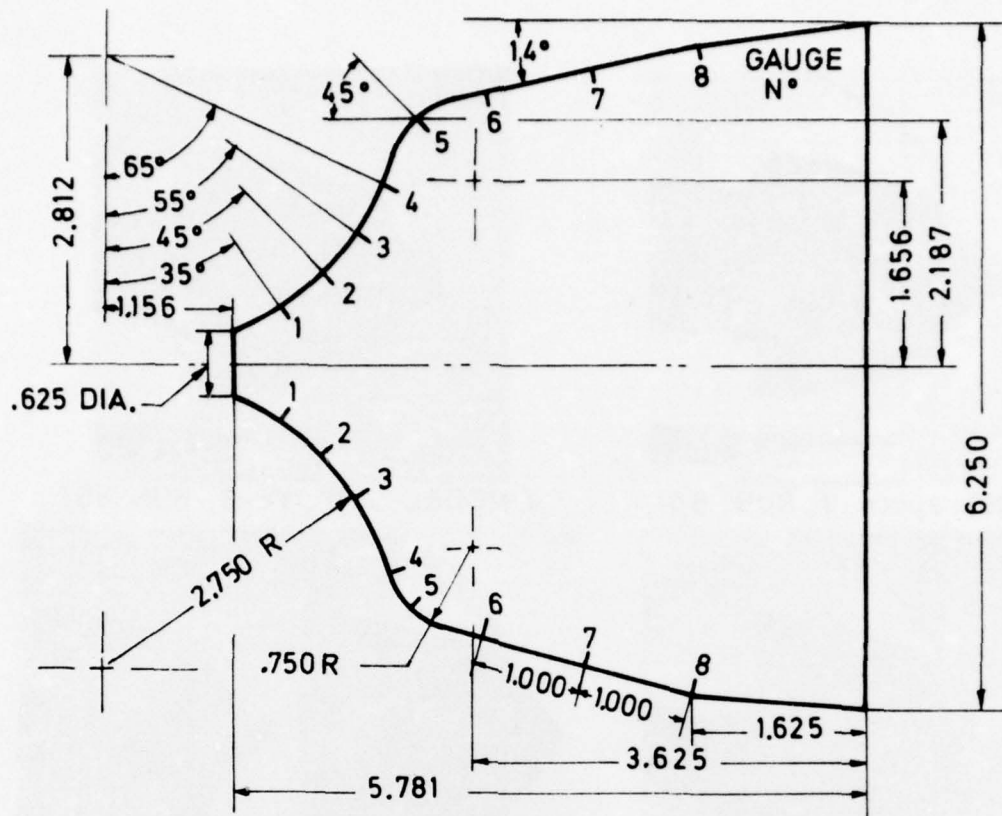
TABLE 5 HEAT TRANSFER MEASUREMENTS (B.Th.U./ft<sup>2</sup>sec)

M	$Re \times 10^{-6}$	Model	Incidence (degrees)	Run No	Stagn pt.	Gauge 1	2	3	4	5	6	7	8
16.8	8.6	J	0	531	155	59	87	149	145	208	20	-	34
16.1	8.3	J	+3	551	130	103	173	333	398	70	25.3	36.0	25.3
16.2	9.0	J	-3	552	190	48.3	75.8	101	75.6	119	23.0	19.2	13.3
16.8	8.6	J(R)	0	534	132	-	44	144	-	150	2	20	34
17.0	8.5	J(Q)	0	561	182	73.6	93.4	173	214	156	24.2	19.5	10.6
16.4	8.4	J(Q)	+3	553	158	76.7	66.6	423	231	95.9	18.2	27.6	23.7
16.1	8.9	J(Q)	-3	554	153	40.8	56.9	107	107	151	23.6	19.9	16.4
15.6	4.5	J	0	530	141	52	60	116	101	151	15	16	28
15.9	4.9	J(Q)	0	560	184	44.5	46.3	125	153	104	20.8	18.6	16.3
20.7	3.1	J	0	529	126	51	86	230	113	142	11	18	17
19.9	3.0	J	+3	549	122	67.8	146	304	174	44.0	13.9	15.0	10.8
19.6	3.3	J	-3	550	148	36.7	57.7	96.2	116	88.2	12.3	14.1	8.9
20.8	3.1	J(R)	0	533	77	42	56	135	-	86	6	-	14
20.7	3.2	J(Q)	0	557	123	31.8	57.6	163	224	25.1	8.9	15.9	12.4
20.7	3.1	J(Q)	+3	558	137	89.5	137	222	114	35.8	14.6	17.0	12.1
20.5	3.2	J(Q)	-3	559	163	27.9	32.5	65.5	108	68.0	14.5	17.3	11.6
20.6	2.8	J(R)	0	532	97	-	190	260	84	111	4	-	16
19.9	2.0	J	0	535	75	28	49	110	94	88	0.5	8.3	12
19.9	2.1	J(Q)	0	556	91.4	20.3	46.2	107	170	30.5	7.6	12.8	8.6

TABLE 6  
NON-DIMENSIONALISED \* HEAT TRANSFER RATES.

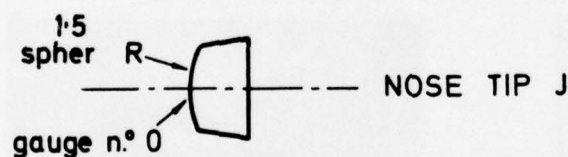
M	$Re \times 10^{-6}$	Model	Inclination (degrees)	Run No	Stagn. point	Gauge 1	2	3	4	5	6	7	8
16.8	8.6	$\tau$	0	531	0.505	0.192	0.283	0.485	0.472	0.678	0.665	-	0.111
16.1	8.3	$\tau$	+3	551	0.427	0.338	0.569	1.023	1.308	0.230	0.053	0.118	0.083
16.2	9.0	$\tau$	-3	552	0.583	0.148	0.232	0.310	0.231	0.366	0.070	0.059	0.041
16.8	8.6	$\tau(Q)$	0	534	0.430	-	0.143	0.469	-	0.489	0.007	0.065	0.111
17.0	8.5	$\tau(Q)$	0	561	0.600	0.243	0.308	0.571	0.706	0.495	0.080	0.064	0.035
16.4	8.4	$\tau(Q)$	+3	553	0.525	0.254	0.220	1.401	0.763	0.317	0.060	0.091	0.078
16.1	8.9	$\tau(Q)$	-3	554	0.479	0.128	0.178	0.334	0.334	0.473	0.074	0.062	0.051
15.6	4.5	$\tau$	0	530	0.603	0.222	0.256	0.496	0.432	0.645	0.064	0.068	0.120
15.9	4.9	$\tau(Q)$	0	560	0.489	0.191	0.198	0.536	0.653	0.445	0.089	0.080	0.070
20.7	3.1	$\tau$	0	529	0.586	0.237	0.400	1.070	0.526	0.660	0.051	0.084	0.079
19.9	3.0	$\tau$	+3	549	0.530	0.307	0.659	1.374	0.788	0.198	0.063	0.068	0.049
19.6	3.3	$\tau$	-3	580	0.607	0.151	0.237	0.396	0.478	0.363	0.051	0.058	0.037
20.8	3.1	$\tau(Q)$	0	533	0.360	0.196	0.243	0.631	-	0.402	0.028	-	0.065
20.7	3.2	$\tau(Q)$	0	557	0.537	0.339	0.251	0.710	0.978	0.109	0.039	0.069	0.054
20.7	3.1	$\tau(Q)$	+3	558	0.599	0.391	0.599	0.968	0.496	0.156	0.064	0.074	0.053
20.5	3.2	$\tau(Q)$	-3	559	0.699	0.120	0.140	0.281	0.463	0.292	0.062	0.074	0.050
20.6	2.8	$\tau(Q)$	0	532	0.475	-	0.931	1.275	0.412	0.544	0.020	-	0.078
19.9	2.0	$\tau$	0	535	0.463	0.173	0.302	0.679	0.580	0.543	0.004	0.051	0.074
19.9	2.1	$\tau(Q)$	0	536	0.479	0.106	0.252	0.362	0.889	0.160	0.040	0.067	0.045

\* with respect to the theoretical stagnation point heat transfer on 0.312 in radius hemisphere (see Table 2)



CONFIGURATION OF THE BASIC BODY

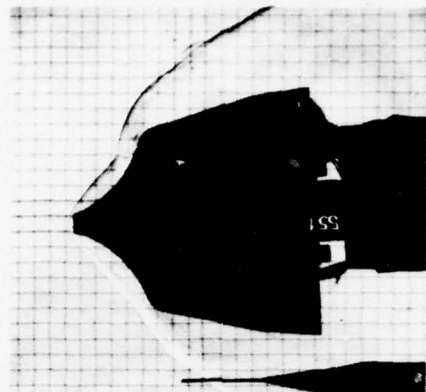
(Note: all dimensions in inches)



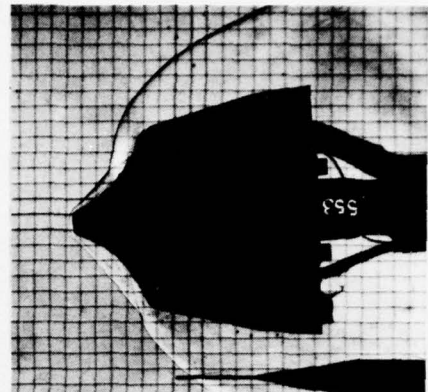
DISTANCE FROM STAGNATION POINT ALONG SURFACE

GAUGE N°	1	2	3	4	5	6	7	8
MODEL J	1.05	1.53	2.01	2.49	3.08	3.74	4.74	5.74

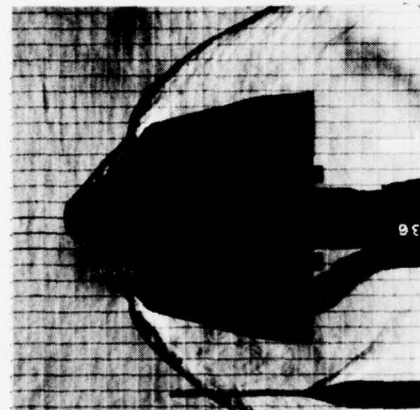
FIG. 1 SCHEMATIC OF BLUNT CONCAVE BICONIC MODEL J



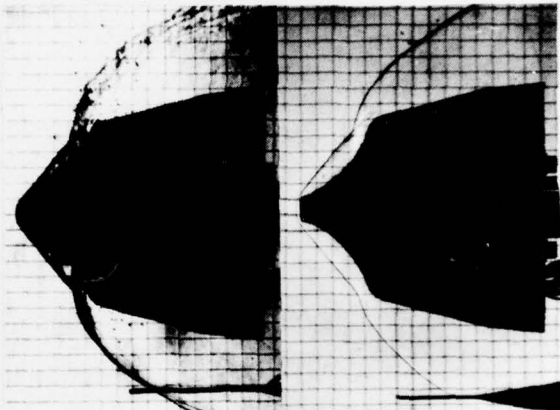
i) MODEL J,  $\alpha = -3$ , RUN 551



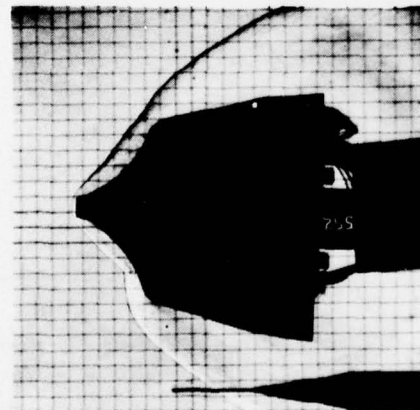
ii) MODEL J(R)',  $\alpha = -3$ , RUN 553



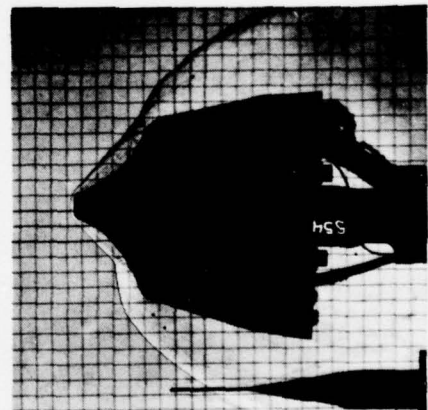
iii) MODEL J,  $\alpha = 0$ , RUN 536



iv) MODEL J(R)',  $\alpha = 0$ , RUN 534, 561



v) MODEL J,  $\alpha = +3$ , RUN 552



vi) MODEL J(R)',  $\alpha = 0$ , RUN 554

FIG. 2a SCHLIEREN PHOTOGRAPHS  $M = 16$ ,  $Re = 9 \times 10^6 / \text{ft}$

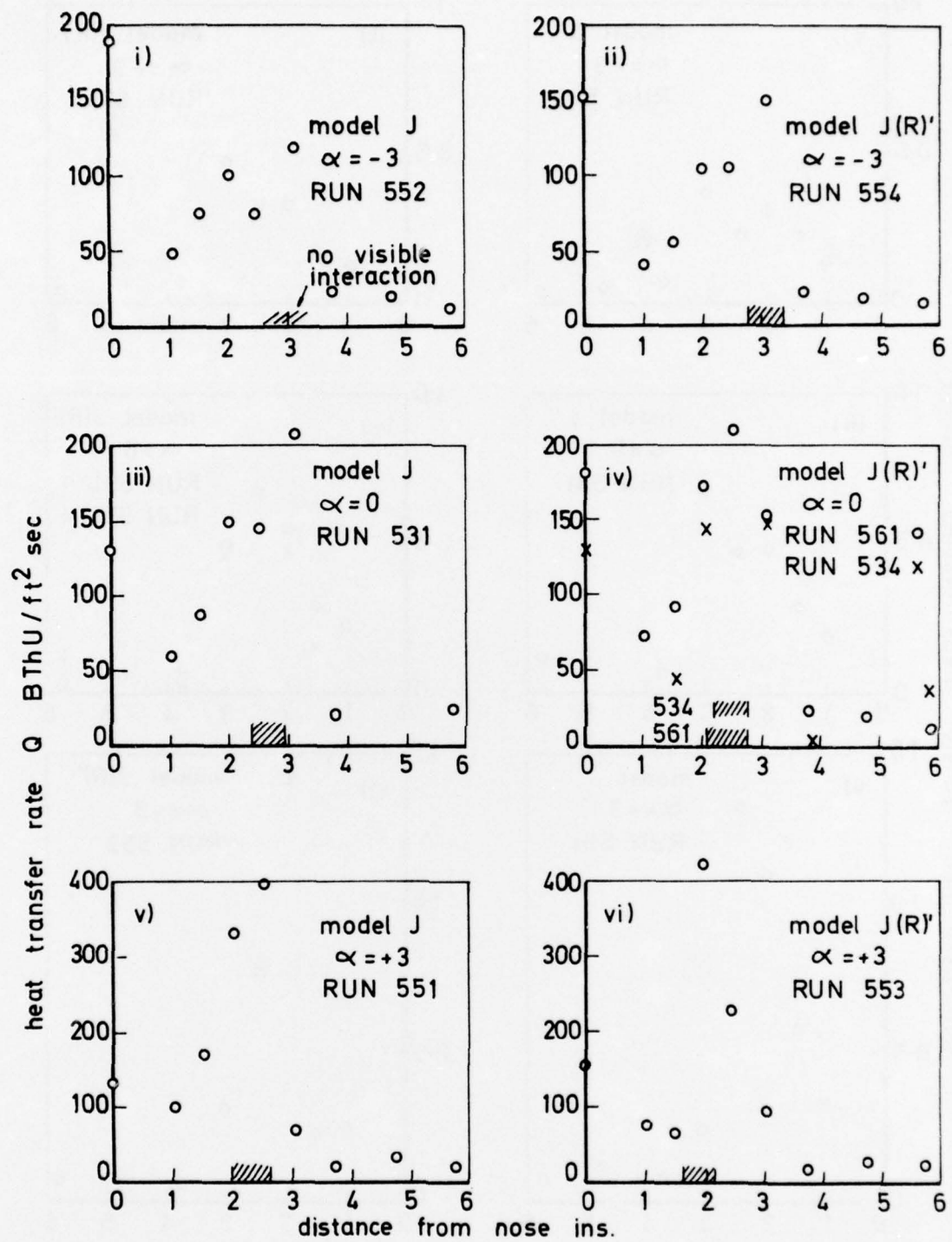


FIG. 2 b. HEAT TRANSFER RATE MEASUREMENTS,  $M=16$ ,  $Re=9 \times 10^6$

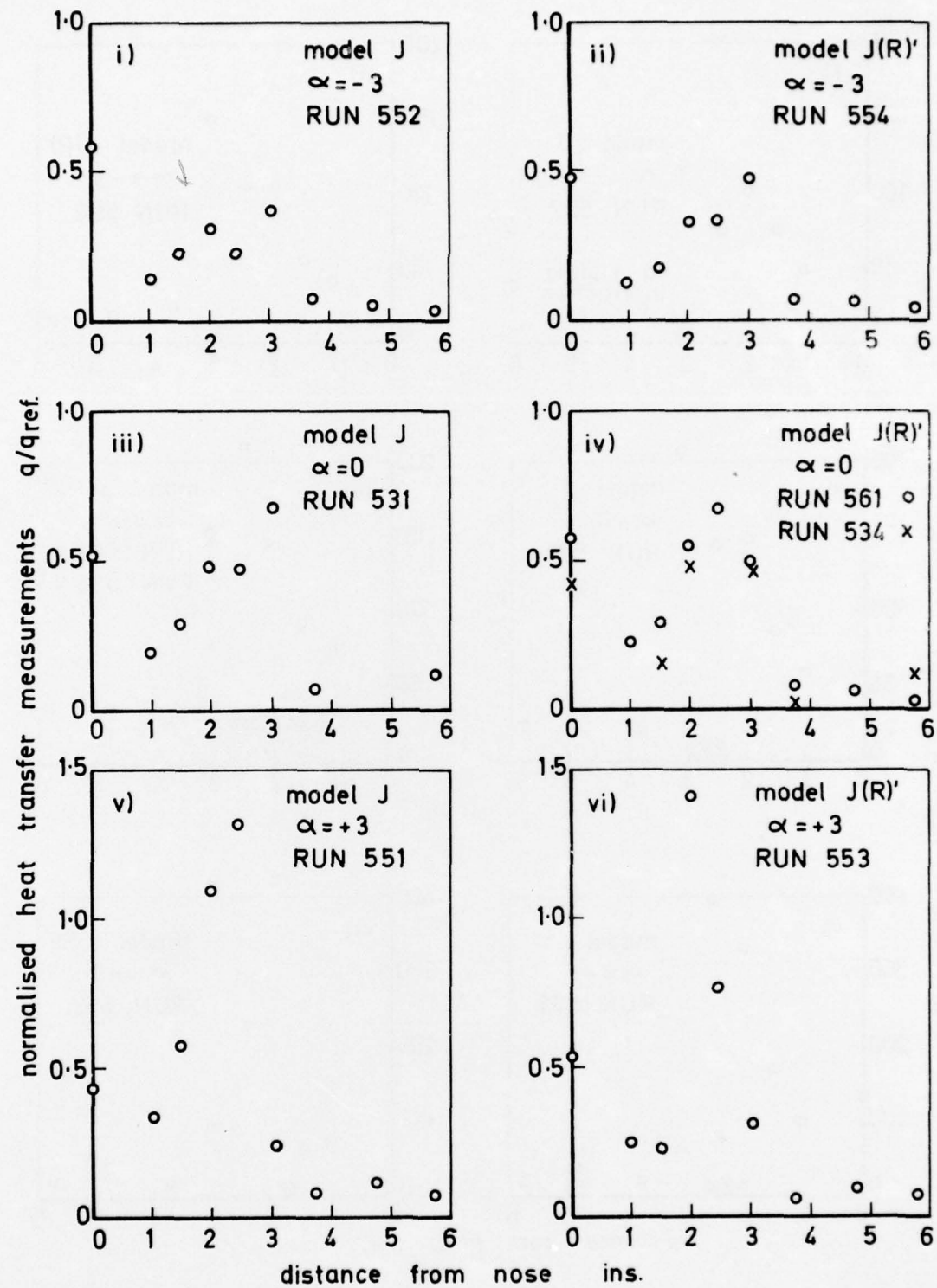


FIG. 2 c. NORMALISED HEAT TRANSFER RATE,  $M=16$ ,  $Re=9 \times 10^6/\text{ft}$

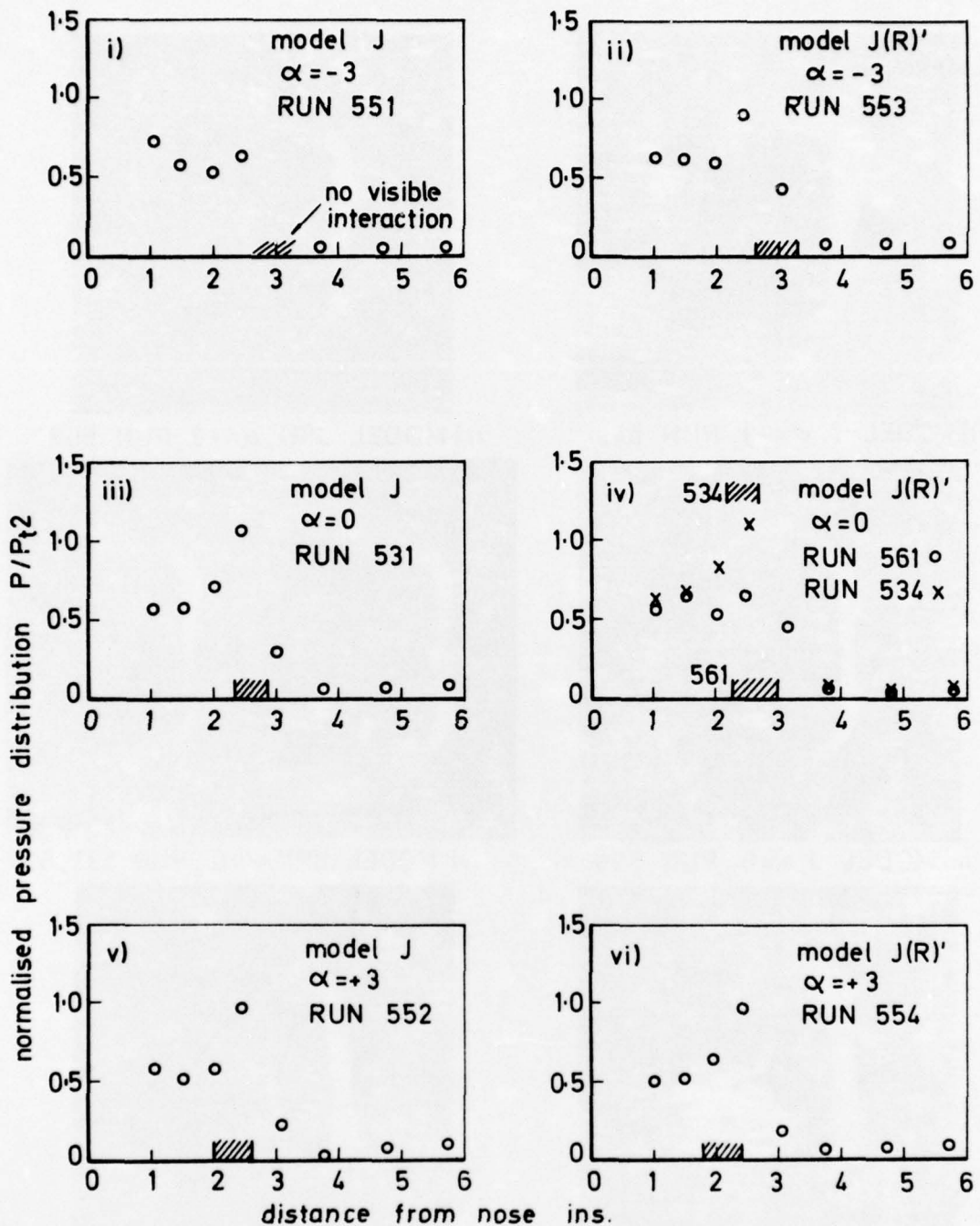
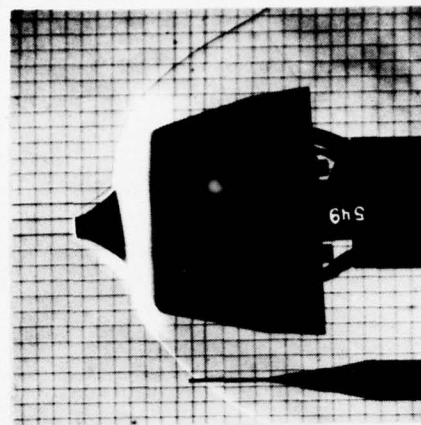
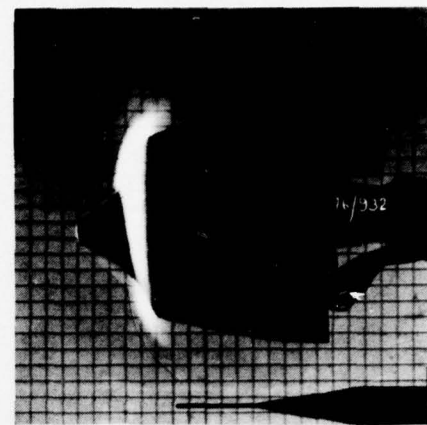


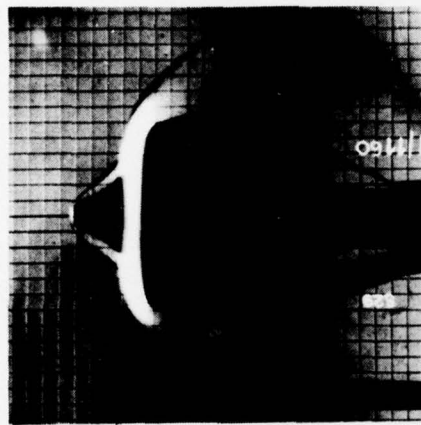
FIG. 2 d. NORMALISED PRESSURE MEASUREMENTS,  $M=16, Re=9 \times 10^6/\text{ft}$



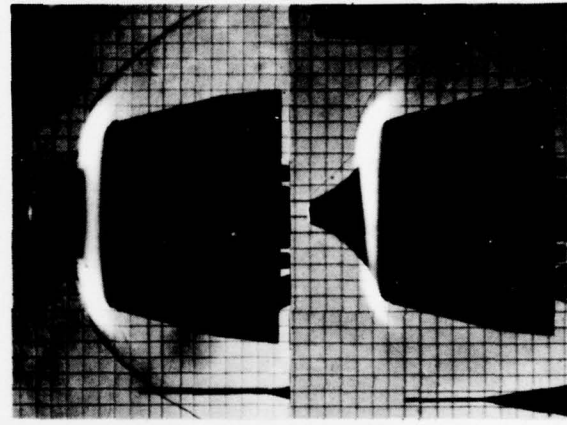
i) MODEL J,  $\alpha = -3$ , RUN 549



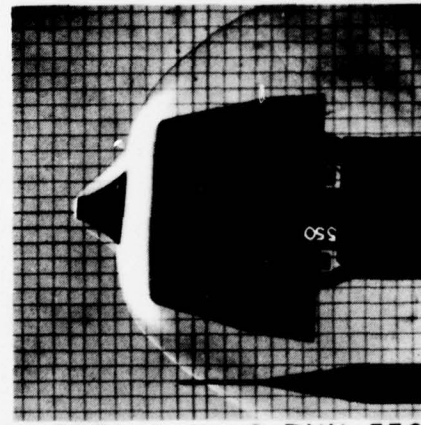
ii) MODEL J(R)',  $\alpha = -3$ , RUN 558



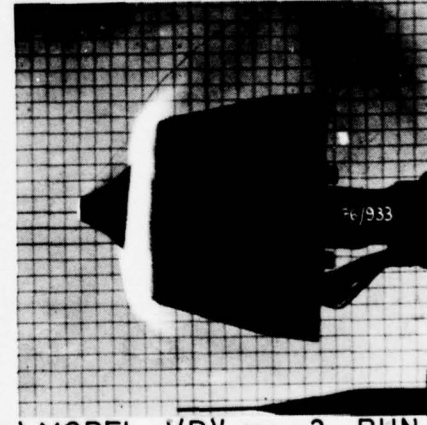
iii) MODEL J,  $\alpha = 0$ , RUN 529



iv) MODEL J(R)',  $\alpha = 0$ , RUN 533, 557



v) MODEL J,  $\alpha = +3$ , RUN 550



vi) MODEL J(R)',  $\alpha = +3$ , RUN 559

FIG. 3a SCHLIEREN PHOTOGRAPHS,  $M = 20$ ,  $Re = 3 \times 10^6 / \text{ft}$

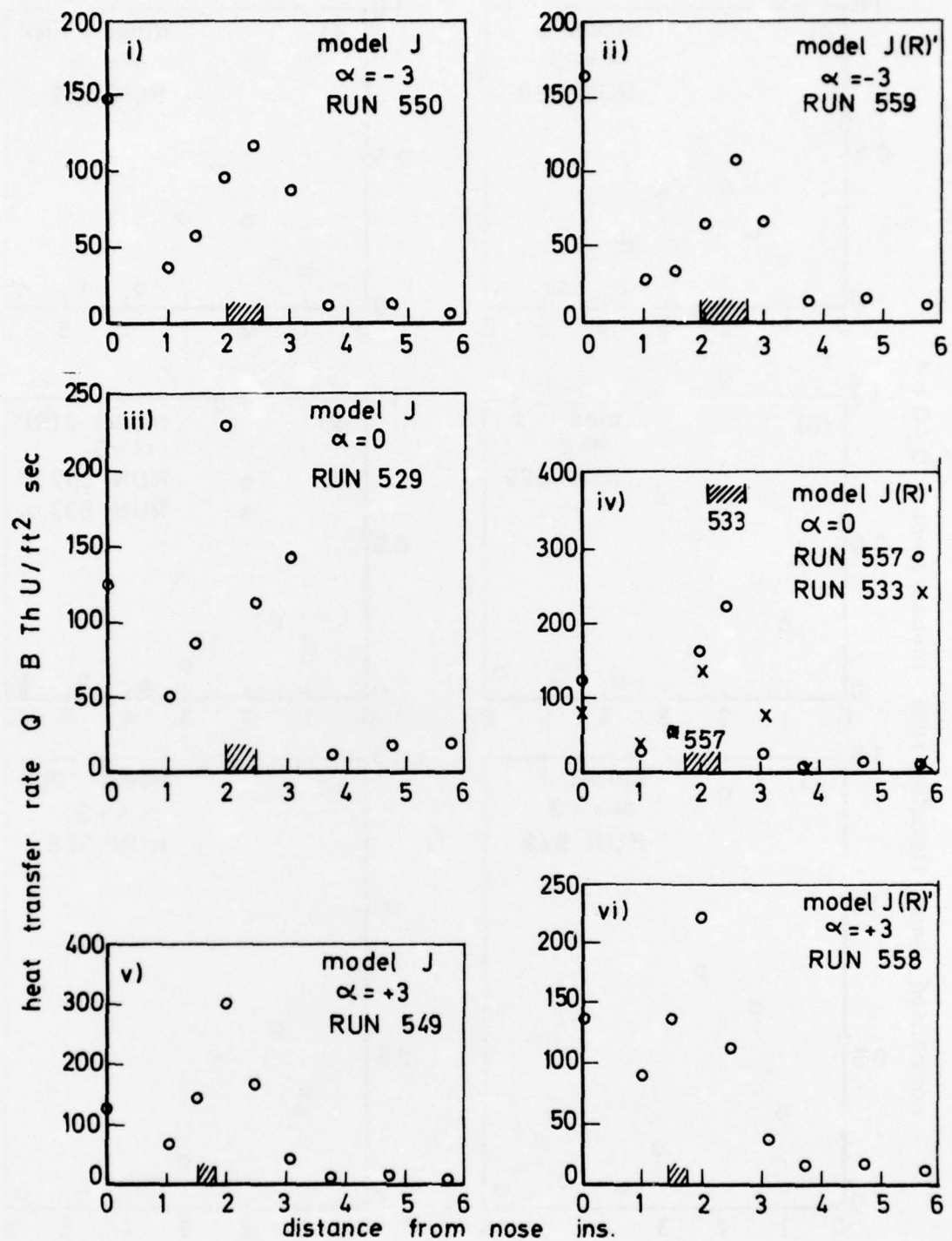


FIG. 3 b. HEAT TRANSFER RATE MEASUREMENTS,  $M = 20$   
 $Re = 3 \times 10^6 / \text{ft}$

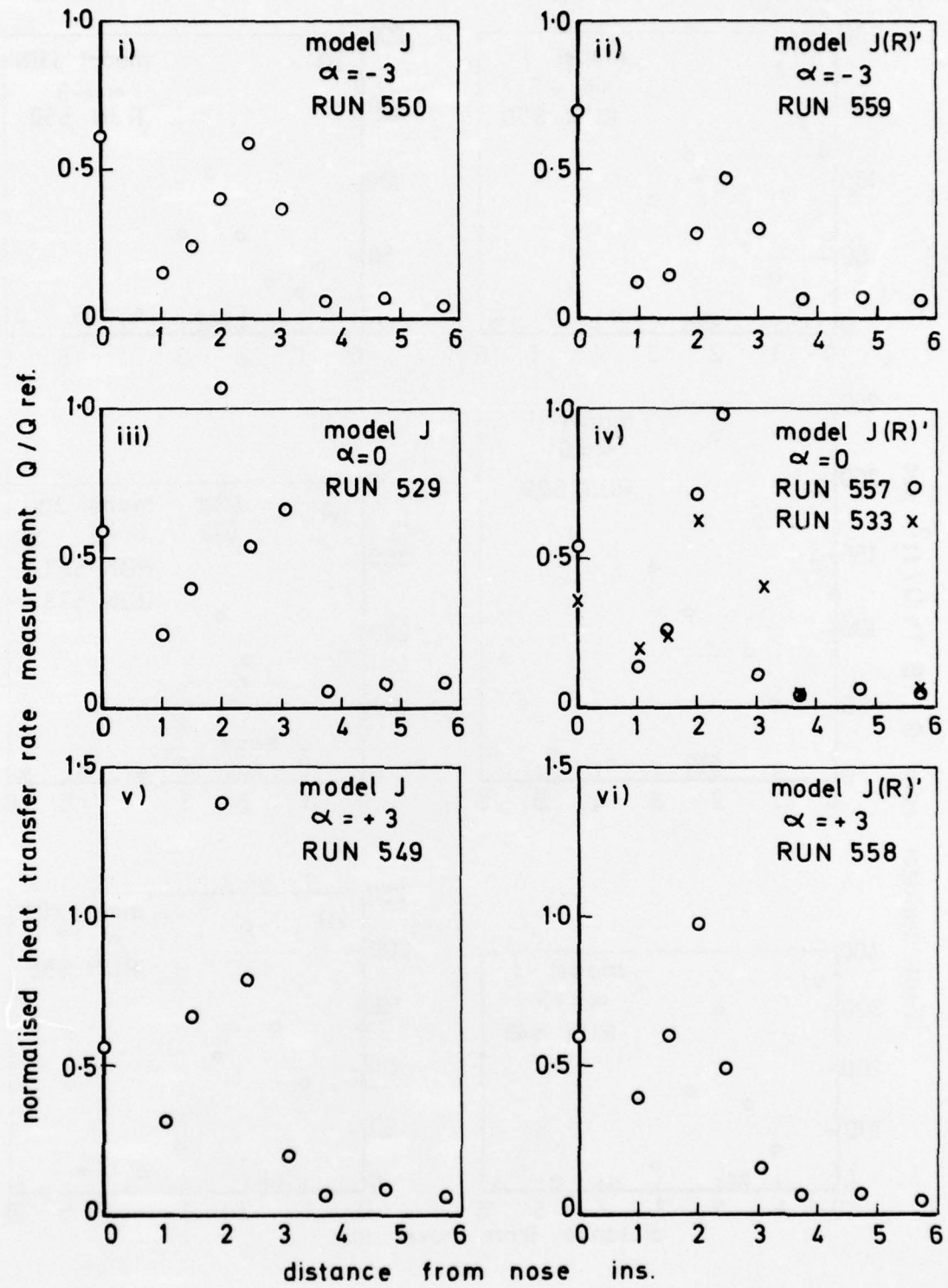


FIG. 3c. NORMALISED HEAT TRANSFER RATE,  $M=20$ ,  $Re=3\times 10^6/\text{ft}$

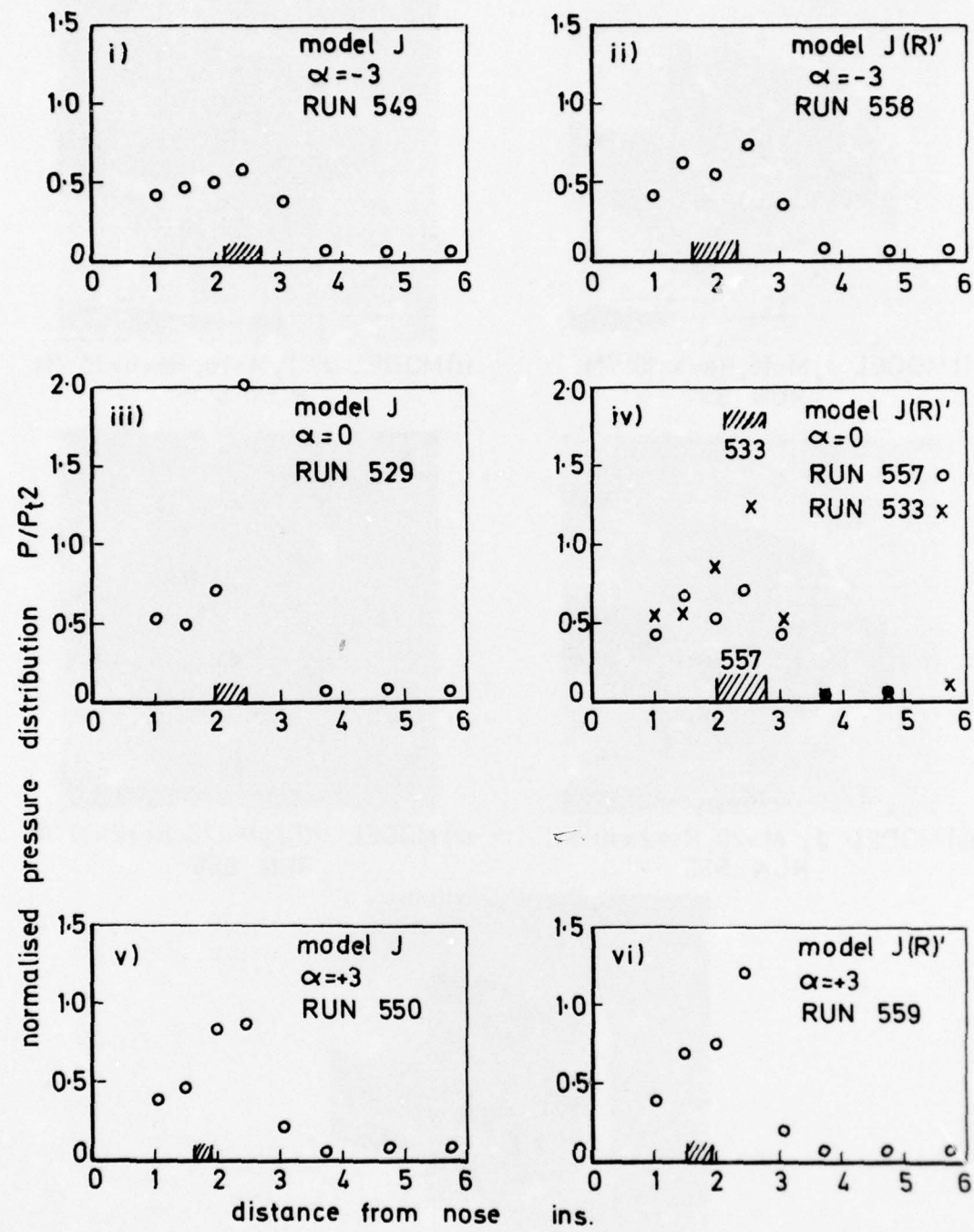
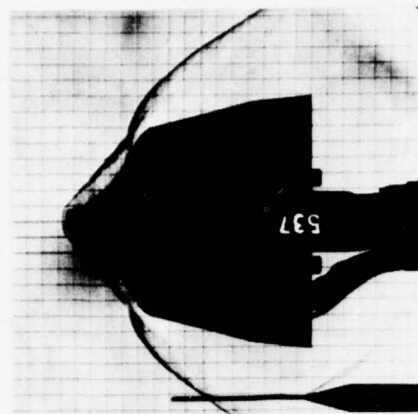
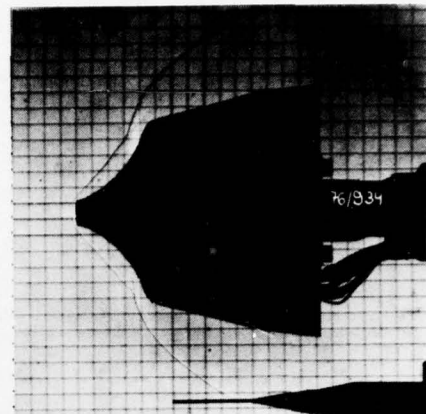


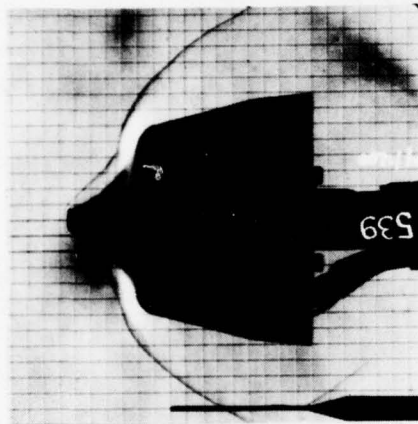
FIG. 3 d. NORMALISED PRESSURE DISTRIBUTION,  $M=20$ ,  $Re=3 \times 10^6$  ft



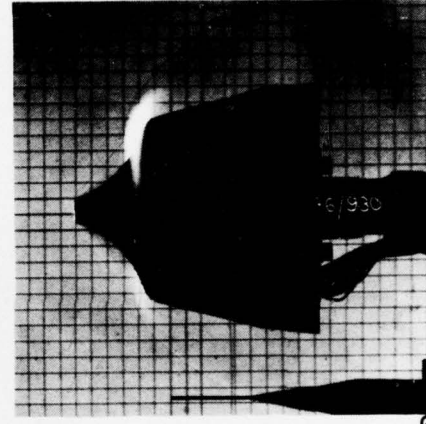
i) MODEL J, M=16,  $Re=5 \times 10^6/\text{ft}$   
RUN 537



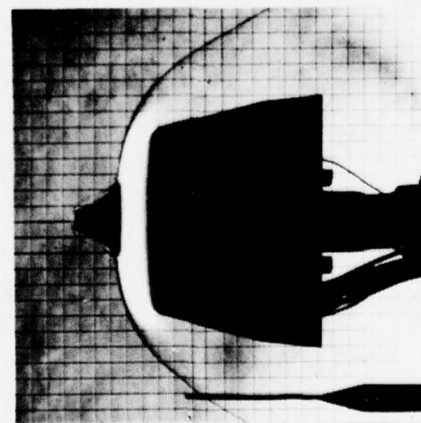
ii) MODEL J(R)', M=16,  $Re=5 \times 10^6/\text{ft}$   
RUN 560



iii) MODEL J, M=20,  $Re=2 \times 10^6/\text{ft}$   
RUN 539



iv) MODEL J(R)', M=20,  $Re=2 \times 10^6/\text{ft}$   
RUN 556



MODEL J(R), M=20,  $Re=3 \times 10^6$   
RUN 532

FIG. 4a. SCHLIEREN PHOTOGRAPHS, ZERO INCIDENCE

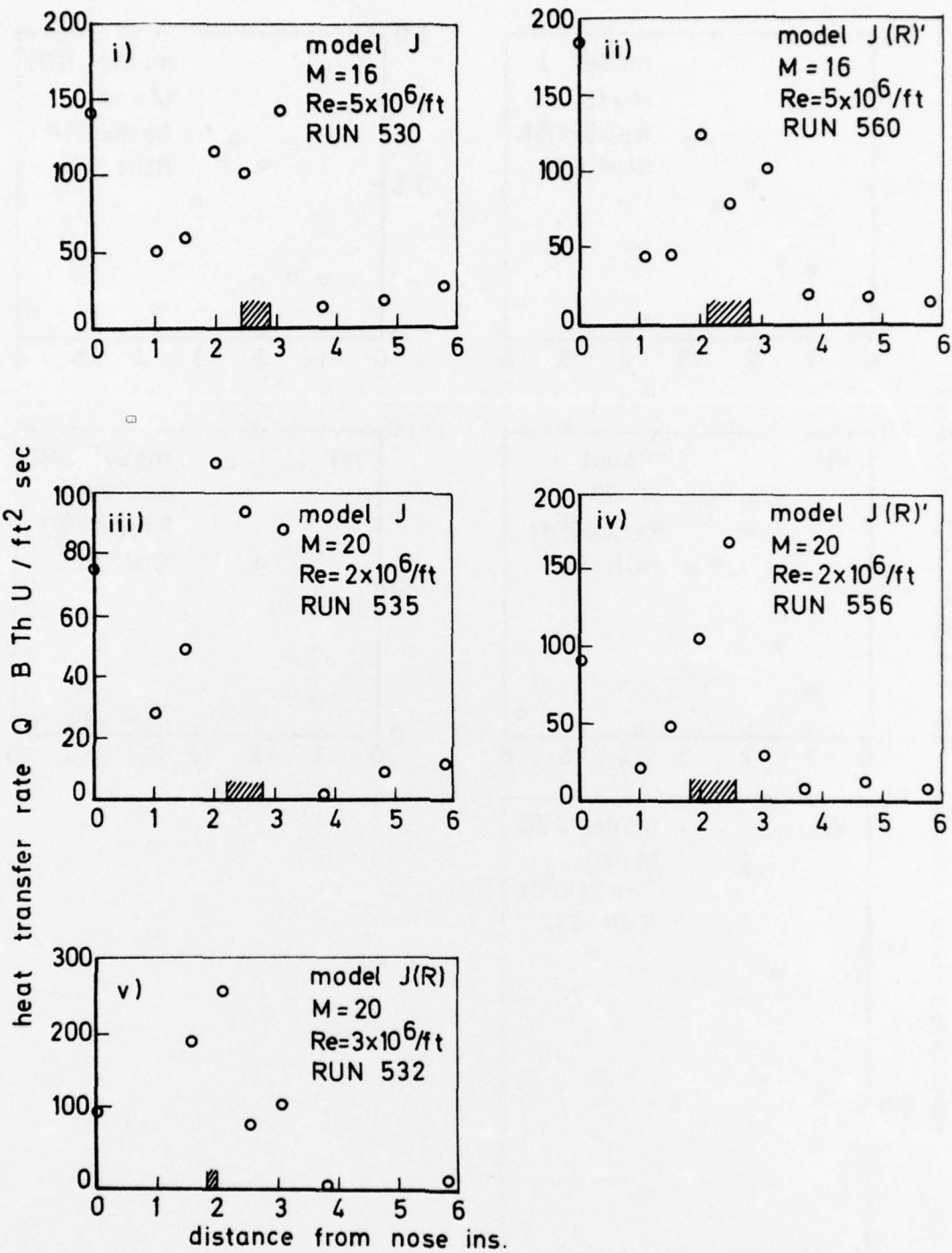


FIG. 4 b. HEAT TRANSFER RATE MEASUREMENTS, ZERO INCIDENCE

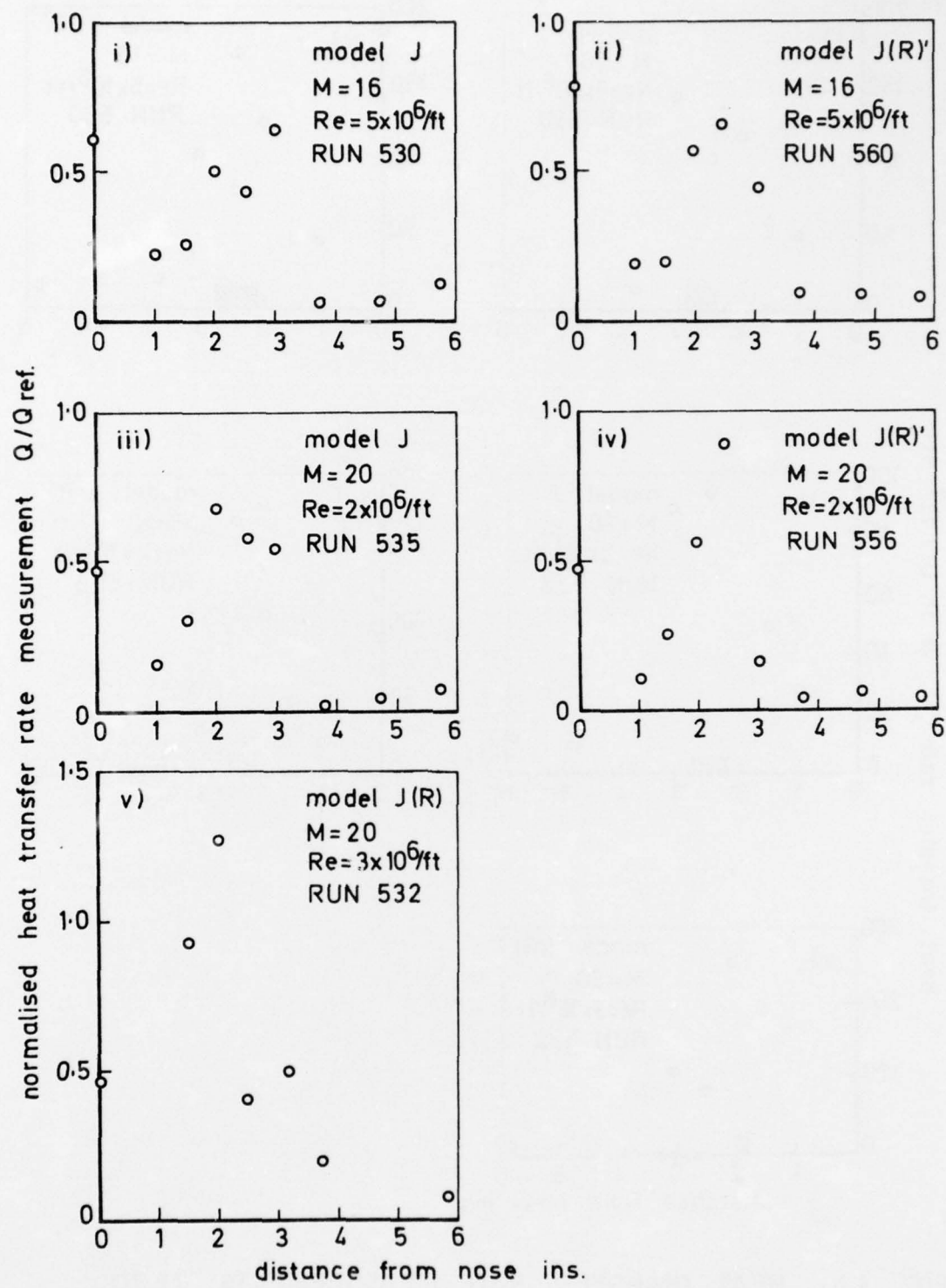


FIG. 4 c. NORMALISED HEAT TRANSFER RATE, ZERO INCIDENCE.

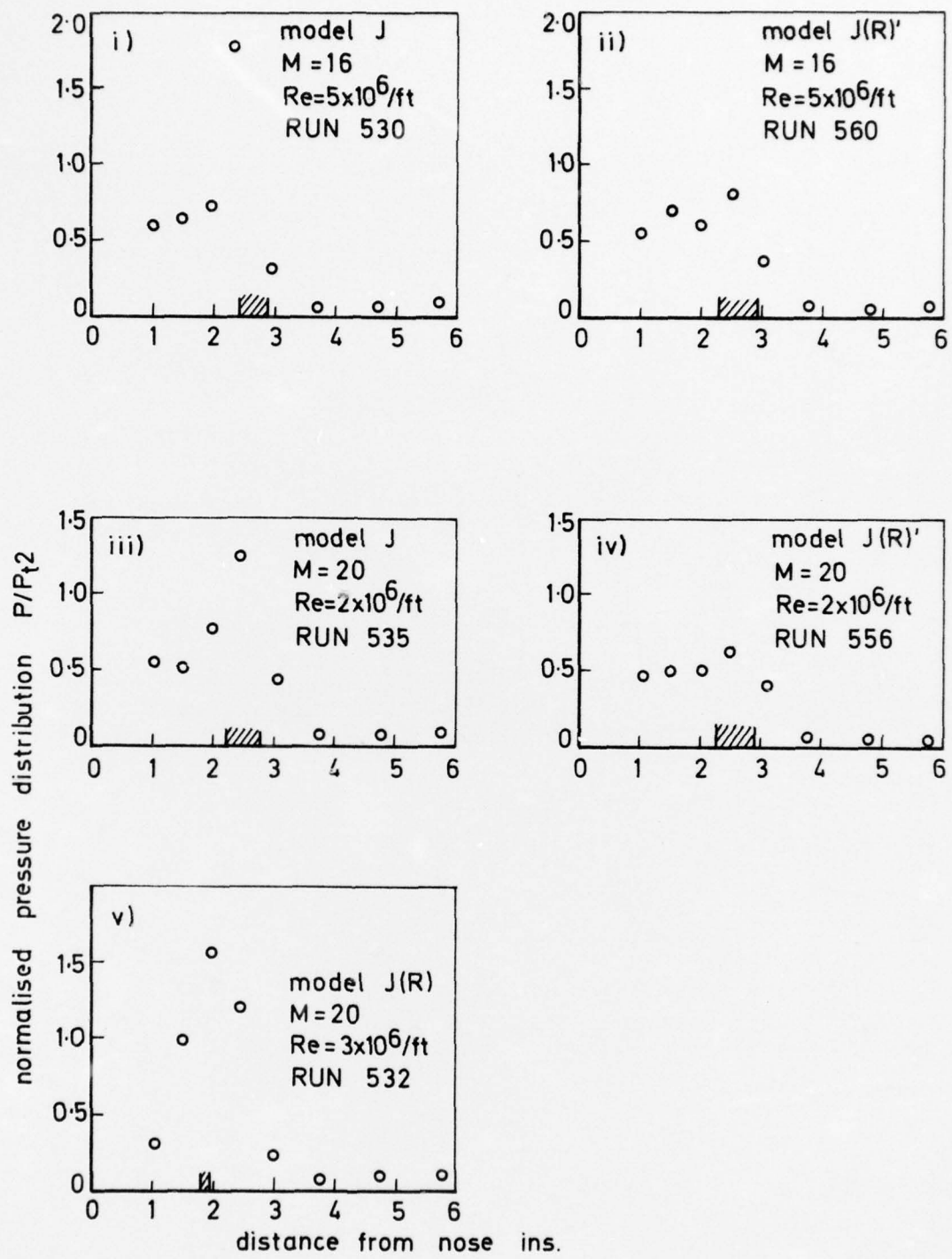


FIG. 4 d. NORMALISED PRESSURE DISTRIBUTIONS, ZERO INCIDENCE

